Article

The Polymorphs of Diacetylcurcumin (DAC)

Marco A. Obregón-Mendoza , Rosario Tavera-Henández , Rubén Sánchez-Obregón , Carolina Escobedo-Martínez , Rubén A. Toscano , Raúl G. Enríquez *

Posted Date: 18 May 2026

doi: 10.20944/preprints202605.1127.v1

Keywords: polymorphism; diacetylcurcumin; DAC

 doi:10.20944/preprints202605.1127.v1

Article

The Polymorphs of Diacetylcurcumin (DAC)

Marco A. Obregón-Mendoza [1], Rosario Tavera-Henández [1], Rubén Sánchez-Obregón [1], Carolina Escobedo-Martínez [2], Rubén A. Toscano and Raúl G. Enríquez [1,*]

[1] Instituto de Química, Universidad Nacional Autónoma de México, Mexico City 04510, Mexico

[2] Departamento de Farmacia, División de Ciencias Naturales y Exactas, Universidad de Guanajuato, Campus Guanajuato, Guanajuato 36050, Mexico

* Correspondence: enriquezhabib@gmail.com

Abstract

Herein, Diacetylcurcumin (DAC), a derivative of curcumin, was synthesised, and two new polymorphs (monoclinic and triclinic) are reported in addition to the previously known polymorph ($P2_1$). Solid-state NMR (CP-MAS) and X-ray studies allowed the unambiguous authentication of the elusive polymorph 2 (canoe-shaped, $P2_1/n$) and the concomitant polymorph **3** (elliptical-shaped, *P-1*). We demonstrate that morphological crystal analysis under a microscope, in conjunction with ATR-IR, is a rapid and inexpensive technique for exploring the polymorphic landscape of curcuminoids. This discovery highlights the ongoing progress in curcumin derivative research and should inspire fellow chemists and materials scientists to further explore it.

Keywords: polymorphism; diacetylcurcumin; DAC

1. Introduction

Polymorphism has been widely understood in the pharmaceutical industry [1] since the crystalline form of a material can be indicative of certain crucial physicochemical properties (e.g. melting point, solubility, thermal stability, etc.) which is of great importance in a legal and patenting sense. However, basic and frontier research is enriched by exploring the subject of polymorphism; at a theoretical level it is important to understand intermolecular interactions, crystal lattice energies [2] or the correction of dispersed bodies so that molecular crystal predictions are more accurate, whistly at an experimental level, the discovery of polymorphs is an exciting challenge (since there is no real recipe) and it is likely that the large investment of "time and money" [3,4] will lead to a better mapping of certain polymorphic landscapes, and in the case of bioactive natural products (or their derivatives) it is important to control the solid state in order to guarantee the biological properties found.

Curcumin or diferuloylmethane [5,6], the natural major curcuminoid [7] extracted from the rhizome of *Curcuma longa* L., is a hydrophobic polyphenolic compound with well-documented biological activities such as antioxidant, anti-inflammatory, anticancer, cytotoxic and anti-disease Alzheimer [8,9]. Poor absorption, low bioavailability and rapid metabolism [10] have hampered the use of curcumin in the clinic. Therefore, the search of polymorphs or the preparation of derivatives by replacement of terminal phenol groups (-OH) has been a strategy to provide new curcuminoids more stable and soluble. When acetate groups take the place of phenols, diacetylcurcumin (DAC) is obtained [11,12] (see Scheme 1).

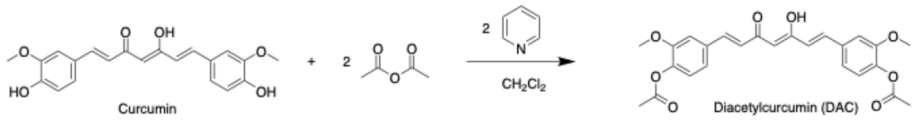

Scheme 1. Synthesis of DAC.

 doi:10.20944/preprints202605.1127.v1

The results of various investigations have shown that DAC can bind to valuable vehicles such as proteins (bovine albumin and alpha-lactalbumin) [13,14], and due to its lipophilicity, DAC has caused an inhibition of inflammation in a murine model [15], thus showing its anti-arthritic activity. Furthermore, DAC has been shown efficacy for scavenger of free radicals (e.g. NO and O_2^-) [16].

The acetyl groups in DAC are less reactive and facilitate biomembrane permeability, which is important since DAC has the potential to be used against resistant bacteria (*S. aureus*) [17]. In addition, when DAC has been tested in antimicrobial photodynamic therapy [18], it has been shown to exhibit greater antimicrobial activity than the parent molecule (curcumin).

The solid-state study of curcumin has led to the discovery of three polymorphs. In 1982, Hjorth Tonnesen *et al.* [19] reported the first crystal structure of curcumin (designated as Form 1, monoclinic, *P2/n*) and ca. of 30 years later (2011) Sanphui *et al.* [20] reported in ChemComm two new polymorphs of curcumin, namely Form 2 (*Pca2₁)* and Form 3 (*Pbca*) and found that orthorhombic (Form 2) exhibits better solubility.

Curcumin Form 1 was obtained in an ethanol (EtOH) solution by adding water as an anti-solvent. Polymorphs 2 and 3 were obtained using a protic polar solvent (EtOH) and the co-formers of crystallisation, 4-hydroxypyridine and 4,6-dihydroxy-5-nitropyrimidine, respectively. Other reports [21–23] have indicated that the three polymorphs can be successfully obtained using chloroform, isopropanol, methanol and dimethyl sulfoxide.

In addition, various experimental methodologies have been established for obtaining curcumin polymorphs. In the 1982 report, slow evaporation and cold solvent for nucleation were used; for the 2011 polymorphs, kneading with a mortar before nucleation was part of the bottom-up approach for polymorphs 2 and 3. Furthermore, it has been reported that the polymorphs were obtained from a supersaturated curcumin solution at various temperatures. In a 2019 manuscript [24] on the relationships among curcumin polymorphs, it is noted that low pressure (100-400 mbar) affects intermolecular interactions and facilitates nucleation. This feedback is important and shows that there is no single recipe for obtaining curcumin polymorphs, since experimentation with a knowledge-driven approach has been key to the different contributions.

DAC has been a promising derivative for the treatment of several human diseases, but the study of its polymorphic landscape has been absent in the literature and only one single crystal structure (monoclinic space $P2_1$, named here as Form-1) has been reported past two decades ago (2004) [25].

Although there is no recipe that guarantees the discovery of polymorphs, herein we have performed a screen for DAC crystals, and three polymorphs (two new ones) have been found and characterised by their single-crystal habits and by thermal analysis. Solid-state by Attenuated Total Reflectance (ATR-IR) and Cross-Polarisation Magic-Angle Spinning Nuclear Magnetic Resonance (^{13}C CP-MAS-NMR) has been used to characterise the non-equivalent carbons. Furthermore, the total certainty of the DAC polymorphs has been established by single-crystal X-ray diffraction.

2. Results

Our approach for bottom-up of DAC and detection of polymorphs was based on the following: a) several solvents with low, intermediate and high dielectric constants were used, b) the choice of the solvents has been based on their protic and aprotic nature, and the experiments were carried out at different temperatures (room and cold) and used of *vacuum* for some cases, c) a visual inspection of the appearance of the single crystals under a microscope optical has been necessary, d) a rapid analysis of the powders in solid state has been carried out by means of spectroscopic techniques (ATR-IR) for each batch, e) to authenticate the polymorphs ^{13}C CP-MASS and X-ray diffraction techniques were used.

DAC was synthesized using acetic anhydride and pyridine as catalyst (see previous reports) [26] and was characterized by liquid NMR ($CDCl_3$), the molecule is a tautomer totally enolized (enol = 16 ppm) which is a characteristic to exert the important reported biological effects, the characterization and spectral assignment is agreement with literature [11,27] and is found in the supplementary information (SI).

 doi:10.20944/preprints202605.1127.v1

The obtaining of DAC single crystals by slow evaporation of solvents under protection from light was carried out at room temperature or under refrigeration (2 °C). It is important to note that under these bottom-up experimental conditions only two polymorphs were obtained (named here Form-1 and Form-3, see Table 1) that were first identified by their different crystalline forms with an optical microscope.

Table 1. Screening of solvents for obtention of crystals of DAC.

Solvent	ε [a]	Temperature	Time (days)	Polymorph observed
Ethyl acetate	6.02	room	3	Form-1
Ethyl acetate	6.02	refrigerator	5	Form-1 and Form-3
Dichloromethane	8.93	room	5	Form-1
Dichloromethane	8.93	refrigerator	10	Form-3
Acetone	20.7	room	2	Form-1
Acetone	20.7	refrigerator	5	Form-3
Ethanol	24.5	room	1	Form-1
Ethanol	24.5	refrigerator	1	Form-1
Methanol	32.7	room	1	Form-1 and Form-3
Methanol	32.7	refrigerator	1	Form-1
Acetonitrile	37.5	room	1	Form-1
Acetonitrile	37.5	refrigerator	3	Form-1 and Form-3

[a] Dielectric constant.

It was observed that the crystals that look like "fine bars" belong to Form-1, while those that look like "elliptical shape" correspond to Form 3. Whereas pure Form-1 (more observed) was present in the majority of the common solvents screening, only in dichloromethane and acetone (where DAC is very soluble), the single crystal of the polymorphic Form-3 was identified. Although under the experimental conditions (see Table 1), the crystalline Form-2 (referred to as elusive polymorph [28]) was not observed, the polymorphic forms 1 (previously reported, CSD code EYIZER01 [29]) and 3 (concomitant polymorph [1]) were also observed in a mixture of single crystals.

The experimental background [30] on obtaining polymorphs 2 and 3 of curcumin allowed us to establish the experimental conditions for the formation of crystalline powders, which were obtained immediately upon crystallisation by mixing solvents [20,31] and rapid cooling *under vacuum*. In this respect, n-hexane (ε = 1.89) or water (ε = 80) was used as an anti-solvent with the application of immediate *vacuum* (200 mbars). For the first attempt, polymorphic Form-2 was successfully obtained (see Table 2), while Form-1 was obtained in the subsequent five attempts. The polymorphic powders were authenticated using ATR-IR analysis, which showed that the carbonyl groups (CH_3-C=O and C=O) exhibited subtle differences in their wavenumbers across the polymorphs (Forms 1, 2, and 3).

Table 2. Immediate nucleation of DAC under solvent mixtures with use of vacuum (200 mbar).

Attempt	Solvent	Anti-solvent	Polymorph
1	Ethyl acetate	Hexane	Form-2
2	Dichloromethane	Hexane	Form-1
3	Acetone	Hexane	Form-1
4	Ethanol	Water	Form-1
5	Methanol	Water	Form-1
6	Acetonitrile	Water	Form-1

The single crystal of polymorph 2 was obtained using ethyl acetate and n-hexane (10%) when the solvent mixture was cooled *in vacuum* (200 mbar) until nucleation of the compound was observed.

 doi:10.20944/preprints202605.1127.v1

The microscopic crystal patterns of the DAC polymorphs are very distinctive and have been used for individual characterization of each single crystal; Figure 1 shows that the "fine bars", "canoes" or "elliptical balls" shapes belong to Forms 1, 2 and 3 respectively.

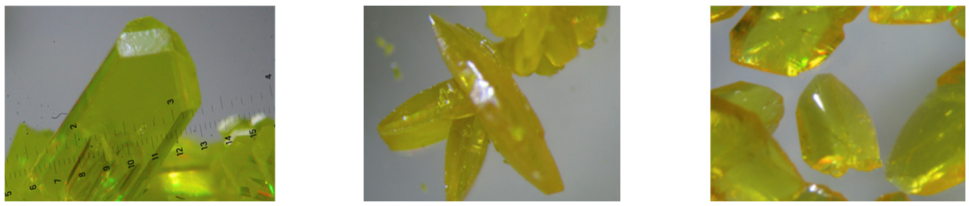

Form-1 Form-2 Form-3

Figure 1. Views of DAC polymorphs (under microscope).

DSC thermograms were obtained for all three polymorphs and are shown in SI, Form 1 (m.p. = 173.89 °C) was found to have the intermediate melting point when compared to Form 2 (m.p. = 164.66 °C) and Form 3 (m.p. = 175.56 °C).

ATR-IR is an advantageous technique [32] for solid state analysis of compounds, since a minimum sample quantity (on average 1 mg) is needed and no preparation prior to analysis is required, and it is also a very economical technique for many determinations. With that in mind, DAC crystals and each batch obtained (see Table 1 and 2) were analysed by ATR-IR spectroscopy (see SI), which were mainly differentiated by the signals belonging to the carbonyl groups (see Table 3).

Table 3. Representative signals of carbonyl groups of DAC polymorphs by ATR-IR.

Carbonyl group (C=O)	Form-1 cm^{-1} (intensity)	Form-2 cm^{-1} (intensity)	Form-3 cm^{-1} (intensity)
Acetate moiety	1756 (strong)	1752 (strong)	1762 (strong)
Keto moiety	1629 (medium)	1625 (medium)	1633 (medium)

Also, differentiation of polymorphs has been made with the ^{13}C CP-MASS NMR determinations. Surprisingly, the non-equivalent carbons are observed as well-defined singlets and no signals broadening is observed because they are crystalline materials [33] and not amorphous (see Figure 2).

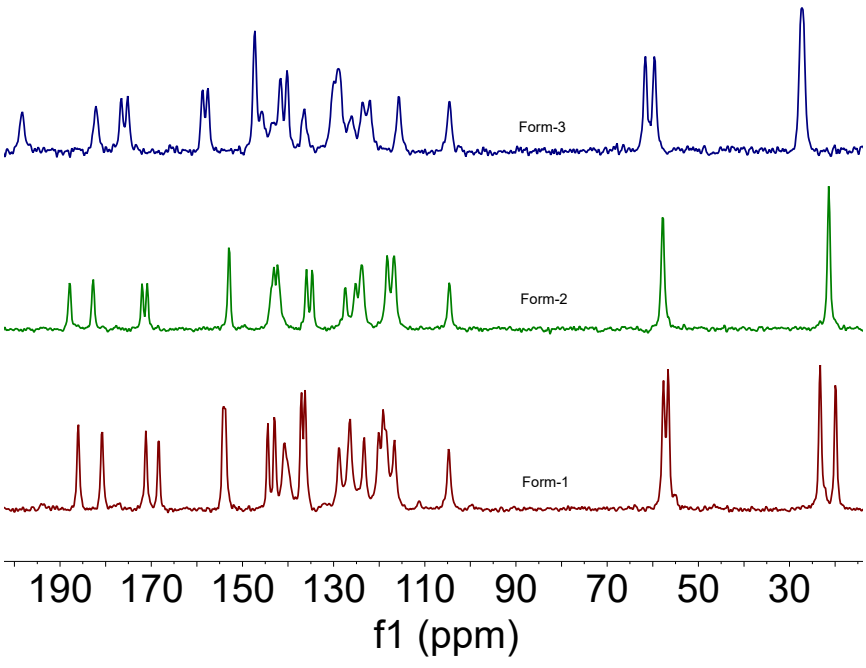

Figure 2. ^{13}C CP-MASS NMR spectra of DAC polymorphs.

 doi:10.20944/preprints202605.1127.v1

The three distinct crystal forms observed were authenticated using the single-crystal X-ray technique, and full crystallographic data for the DAC polymorphs are provided in SI and Table 4, showing that the unit cell parameters are indicative of a clear difference between each polymorph.

Table 4. Crystal parameters of DAC polymorphs.[a]

Property	Form-1	Form-2	Form-3
Space group	*P* 2_1	*P* 2_1/n	*P*-1
a/Å	8,8478(2)	11,4469(19) (19)	9,1473(2)
b/Å	7,9351(2)	10,9829(18) (18)	10,3385(3)
c/Å	16,4135(4)	18,728 (3)	13,2791(3)
α/°	90,00	90,00	78,850(1)
β/°	98,564(1)	99,863 (3)	89,336(1)
γ/°	90,00	90,00	66,556(1)
Volume/ $Å^3$	1139,51(5)	2319,7(7)	1127,4(1)
D_{calcd}Mg m^{-3}	1.319	1.296	1.333
Z	2	4	2
$R_1[I>2\sigma(I)]$	0.0402	0.0539	0.0564
wR_2 (all)	0.1024	0.1528	0.1580
Goodness-of-fit	1.079	1.014	1.027

[a] Full crystal data is given in SI.

The solubility of the polymorphs was measured in a water-ethanol (40%) mixture (see SI), finding that polymorphic Form-2 (less stable) was more soluble than Form-3 (more stable), which agrees with the literature reporting an inverse relationship between stability and solubility [24].

3. Discussion

Diacetylcurcumin (DAC) was characterised by liquid NMR in $CDCl_3$. The hydrogen spectrum (see SI) showed two singlets corresponding to the terminal acetate (2.31 ppm) and methoxy groups (3.86 ppm) of the aromatic rings. Additionally, two double signals at 6.54 ppm and 7.60 ppm with *trans* coupling constants (15.8 Hz) were observed, corresponding to the vinyl groups of the heptanoid carbon chain. The central methine proton was detected at 5.83 ppm, and aromatic protons were observed between 7.04 ppm and 7.14 ppm in solution. This compound exhibits keto-enol equilibrium [34]. The purity of the DAC was 99.6% as determined by HPLC (see supplementary information), and the DART+ mass spectrum showed a peak with 100% intensity at m/z 453 (see SI) that is consistent with the molecular formula $C_{25}H_{24}O_8$.

A differential scanning calorimetry (DSC) study revealed three distinct melting points for each DAC polymorph: **1** (173.89 °C), **2** (164.66 °C), and **3** (175.56 °C) (see SI). While these data are consistent with the literature [11,15,16,35–37], the polymorphism of DAC had not been previously considered. Therefore, further heating, cooling, and reheating studies were conducted using DSC to confirm the polymorphic relationship (enantiotropic or monotropic) of DAC. DSC analysis of polymorphs 1 and 3 shows different endothermic peaks (155.52 °C and 142.4 °C) before the melting point, but neither corresponds to a transition between polymorphs. Forms 1 and 2, as well as forms 1 and 3, were determined to have a monotropic relationship, as no reversibility was observed between them.

It is important to note that the DSC thermogram of Form 3 (see SI) showed reversibility to Form-2 upon reheating. During the initial heating, an endothermic peak was observed corresponding to the melting point of Form-3 (175.56 °C), and during cooling, the exothermic transition point occurred at 126.45 °C. Upon reheating, an endothermic peak was observed at 166.35 °C, corresponding to the melting of Form-2. Therefore, it is appropriate to conclude that Forms **2** and **3** are enantiotopically related [24].

Determination of polymorphs by the X-ray diffraction technique has been considered the gold standard for the authentication of compounds in the solid state. However, obtaining a single crystal

 doi:10.20944/preprints202605.1127.v1

is problematic in some cases, meaning that the issue of polymorphism is often overlooked. Therefore, the ATR-IR technique [32] is particularly important in this research. Form **2** showed a signal at the lowest wavenumber (1752 cm^{-1}) for the carbonyl groups of acetates (symmetric stretching), which correlates with the high molecular symmetry of DAC. While Forms **1** and **3** show a medium-intensity signal with the highest wavenumbers at the carbonyl group (C=O, region corresponding to the keto-enol fraction, symmetric carbonyl stretching), Form **2** shows it as a band with the lowest wavenumber.

ATR-IR analysis has shown that the bands with the most distinctive characteristics correspond to the carbonyl groups of the acetate fraction and have served to differentiate the three DAC polymorphs. This characteristic can be attributed to the strong interactions among acetate groups as occurs in the crystal lattice of Form-2.

The DAC polymorphs were also analyzed by solid-state NMR. Forms 1 and 3 showed a greater number of signals characteristic of non-equivalent carbons (see Table 5), corresponding to methyl (CH_3-), methoxy (-OCH_3), acetate (-COO-), and carbonyl (C=O) groups, as described below. In contrast, form **2** shows fewer signals because the molecule contains more symmetric carbons.

Table 5. ^{13}C CPMASS of DAC polymorphs, chemical shifts in ppm.

^{13}C	Form-1	Form-2	Form-3
-CH_3	23.31, 19.89	21.38	27.27
-OCH_3	57.65, 56.63	57.79	61.61, 59.61
-COO	171.17, 168.37	172.00, 170.88	176.57, 175.18
-C=O	186, 180.79	187.87, 182.74	198.30, 182.14

The differences in chemical shifts of ^{13}C between the carbonyl groups (*i.e.*, $\Delta\delta(^{13}C) = \delta(^{13}C{=}O) - \delta(^{13}C{=}O)$) revealed that polymorph 3 is the most unsymmetric compound (showing the largest difference $\Delta\delta(^{13}C)$ = 16.16 ppm) followed by polymorphs 1 and 2. Furthermore, these data suggest that Form-2 aper polimorfos DAC and confirmed by ATR-IR and X-ray analysis.

The keto-enol equilibria of DAC polymorphs are preserved in forms 1 and 3, whistly Form-2 showed a symmetric bond type RAHB (C=O···H···O=C) which is depicted in Figure 3. This is indicative that the chemical shift of enolised proton would be about 17.5-18.0 ppm in solid-state NMR, which agrees with a previous study [38]. The bond distances for the keto-enol moiety of the polymorphs were obtained from X-ray analysis, and the structural variations are clearly evident. Form-3 presents an H···O bond length less than 1 Å, which is described to a greater degree as a keto-enol model.

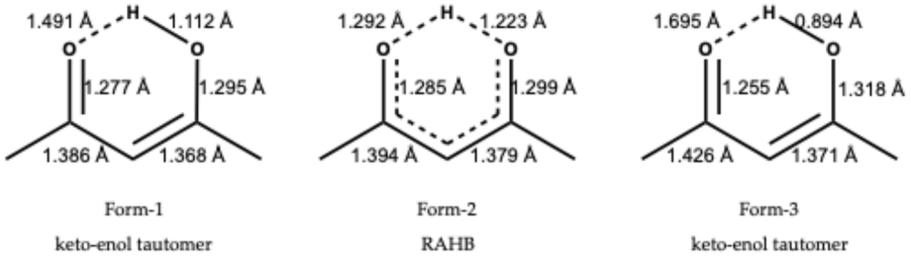

Figure 3. Bond distances of the keto-enol moiety of DAC polymorphs.

Moreover, the difference obtained between C=O and C-O bond length is 1.318 — 1.255 = 0.063 Å for Form-3, and 0.018 Å (Form-1), and 0.014 Å (Form-2) which is representative of unsymmetric, thus greater difference is for the more unsymmetric polymorph (Form-3).

The crystal structure of Diacetylcurcumin (DAC) Form-1 was solved in monoclinic space group $P2_1$ with one molecule in the asymmetric unit (Z' = 1). The molecule exists in the β-keto–enol tautomer [((1*E*,3*Z*,6*E*)-5-hydroxy-3-oxohepta-1,3,6-triene-1,7-diyl) bis (2-methoxy-4,1-phenylene)diacetate] with strong intramolecular hydrogen bond O2−H2A ··· O1, 1.63(4) Å, 2.535(3) Å, 148(4)°. Form-1 molecules adopt a fully-extended linear structure with a curved, slightly twisted conformation. Phenyl rings at both terminals of the molecule are slightly twisted relative to each other, with both

 doi:10.20944/preprints202605.1127.v1

methoxy groups coplanar with the phenyl rings and oriented *syn* to the central keto−enol group. The acetate moieties are nearly perpendicular to the phenyl rings (71.50 and 75.68°) and oriented to opposite sides of the molecule. Weak C–H···O interactions (C15–H15···O8-x+2,y-1/2,-z+2): 2.40 Å, 3.280(4)Å, 157.5°; C20–H20C···O5(-x-1,y+1/2,-z+1): 2.66 Å, 3.486(5) Å, 144.6° and C22–H22C···O7(-x,y+1/2,-z+2): 2.64 Å, 3.500(4) Å, 150.0°) also play an important role in the overall molecular aggregation. Several samples - although not exhaustively- were tested and in all cases, included the report in CSD CODE: EYIZER01 [29] display the same absolute structure showed in Figure 4a.

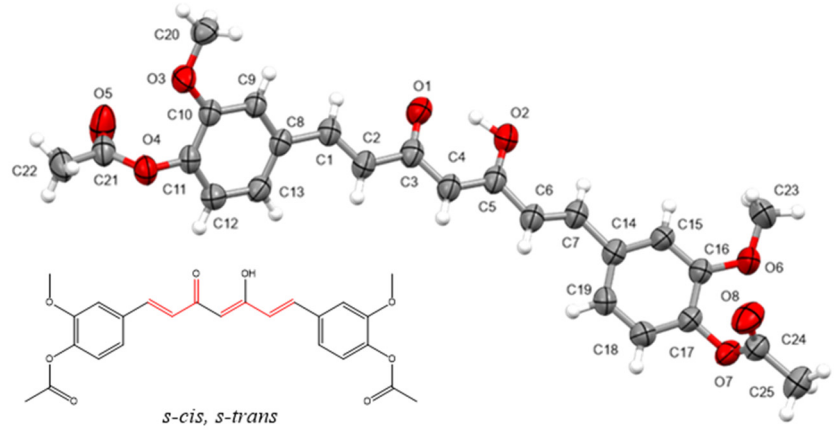

a)

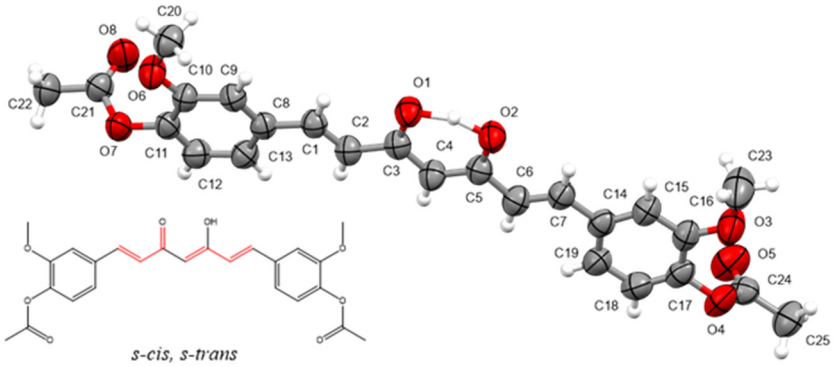

b)

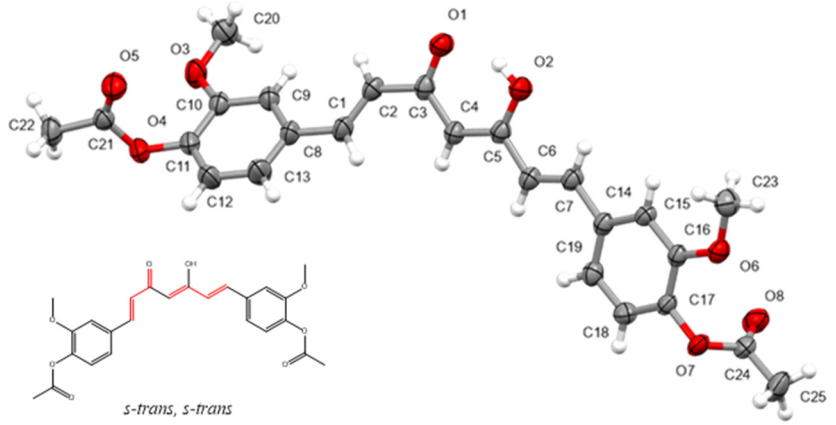

c)

Figure 4. ORTEP diagram of Diacetycurcumin (a) Form-1, (b) Form-2 and (c) Form-3 at 50% probability of electron density for thermal ellipsoids.

 doi:10.20944/preprints202605.1127.v1

The crystal structure of DAC Form-**2** was solved in the monoclinic space group $P2_1/c$ with one molecule in the asymmetric unit (Z' = 1). As found for Form-1 the molecule exists also in the β-keto–enol tautomer [((1*E*,3*Z*,6*E*)-5-hydroxy-3-oxohepta-1,3,6-triene-1,7-diyl) bis (2-methoxy-4,1-phenylene)diacetate] with an even stronger intramolecular hydrogen bond O2−H2A ··· O1, 1.29(3)Å, 2.466(2)Å, 157(3)°. In contrast with the Form-1 molecule, the overall conformation is nearly planar with the acetate moieties almost perpendicular to the phenyl rings (76.64 and 82.31°) but now oriented toward the same side of the molecule (Figure 4b). There are C−H···O interactions from methoxy and the acetoxy groups of one of the phenyl rings (C20−H20B···O2(2 x+1/2,-y+1/2,z+1/2): 2.57 Å, 3.243(3) Å, 127.6°, C22−H22B···O5(x+1,y,z+1): 2.46 Å, 3.416 (4) Å, 172.6° and C22−H22C···O1(-x+3/2,y+1/2,-z+3/2): 2.49 Å, 3.433(3)Å, 166.0°) in addition to the C−H···O interaction C4−H4···O5(x+1/2,-y+3/2,z+1/2): 2.48 Å, 3.342(3) Å, 153.8° from olefinic hydrogens.

The form-**3** crystal structure was solved in the triclinic space group *P-1* and with one molecule in the asymmetric unit. Strong intramolecular hydrogen bond O2−H2A···O1: 1.71(3) Å, 2.5178(17) Å,151(3)° is present in the enol tautomer [((1*E*,3*Z*,6*E*)-5-hydroxy-3-oxohepta-1,3,6-triene-1,7-diyl) bis (2-methoxy-4,1-phenylene)diacetate]. In contrast to forms **1** and **2**, Form-3 molecules adopt a folded L-type conformation. The orientation of the acetate moieties is again almost perpendicular to the phenyl rings (77.32 and 80.73°) but now oriented toward the opposite side of the molecule as found in Form-1 (Figure 4c). There are C−H···O interactions from methoxy and the acetoxy groups of one of the phenyl rings: C20−H20C···O5(-x+1,-y+2,-z+1): 2.63 Å, 3.407(2) Å, 138.9°, C22−H22A···O1(-x+1,-y+2,-z+1): 2.54 Å, 3.494(2) Å, 173.1° and three involving olefinic and aromatic hydrogens C2−H2···O5(-x+1,-y+2,-z+1): 2.59 Å, 3.515(2)Å, 172.5°, C9−H9···O5(-x+1,-y+2,-z+1): 2.60 Å, 3.494(2) Å, 146.2° and C15−H15···O8(-x-1,-y+1,-z): 2.47 Å, 3.305(2)Å, 149.8°.

Torsional flexibility inside the polymorphs suggests that Diacetylcurcumin exists as conformational polymorphs [39,40] (Table 6). Based on the orientation of $-OCH_3$ groups with respect to the central keto−enol group, these conformers can be described as *syn-syn*. A notable feature for Form-3 is the arrangement of its C1−C2−C3−O1 fragment (Figure 4c), with C1 oriented *trans* to O1 (*s-trans* configuration) contrary to the observed *s-cis* configuration for forms 1, and 2. In all structures, the C4−C5−C6−C7 atoms fragment is nearly planar and has an all-*trans* arrangement (*s-trans* configuration) Figure 4 and Table 6. Besides the high degree of planarity, there is a notable absence of OBJ···OBJ stacking between molecules, as confirmed using the Aromatics Analyser component of Mercury program; the separation between the ring centroids exceeds the range of phenyl···phenyl interaction in all cases.

Table 6. Selected bond lengths [Å] and angles [°] for Forms 1-3.

Bond	Form-1	Form-2	Form-3
O(1)-C(3)	1.286(4)	1.286(3)	1.254(2)
O(1)-H(2A)	-------	1.29(3)	----------
O(2)-C(5)	1.293(4)	1.297(3)	1.318(2)
O(2)-H(2A)	1.00(4)	1.23(3)	0.88(3)
C(8)-C(1)	1.470(4)	1.457(3)	1.472(2)
C(1)-C(2)	1.323(4)	1.326(3)	1.312(3)
C(2)-C(3)	1.459(4)	1.452(3)	1.480(2)
C(3)-C(4)	1.395(4)	1.395(3)	1.426(2)
C(4)-C(5)	1.384(4)	1.380(3)	1.371(2)
C(5)-C(6)	1.465(4)	1.451(3)	1.456(2)
C(6)-C(7)	1.323(4)	1.326(3)	1.329(2)
C(7)-C(14)	1.469(4)	1.460(3)	1.472(2)
C(8)-C(1)-C(2)-C(3)	-179.8(3)	-179.9(2)	176.22(18)
C(1)-C(2)-C(3)-O(1)	-14.4(5)	-2.4(4)	-151.80(19)
C(1)-C(2)-C(3)-C(4)	166.0(3)	176.8(2)	27.5(3)
C(2)-C(3)-C(4)-C(5)	178.7(3)	179.5(2)	-174.89(15)
C(3)-C(4)-C(5)-C(6)	-178.1(3)	-179.6(2)	175.47(15)

 doi:10.20944/preprints202605.1127.v1

O(2)-C(5)-C(6)-C(7)	-3.7(5)	-2.8(4)	4.3(3)
C(4)-C(5)-C(6)-C(7)	176.0(3)	177.9(2)	-173.84(16)
C(5)-C(6)-C(7)-C(14)	-180.0(3)	-179.2(2)	176.61(15)

The XPac geometrical analysis of the three polymorphic forms shows that there is no isostructurality, only 1D dimensionality of the common packing fragment is observed between Form-1 and Form-3 (see SI). Molecular overlay (RMSD; **1**vs**2**: 1.391, **1**vs**3**: 1.802, **2**vs**3**: 2.724) of the three polymorphs of Diacetylcurcumin is displayed in Figure 5.

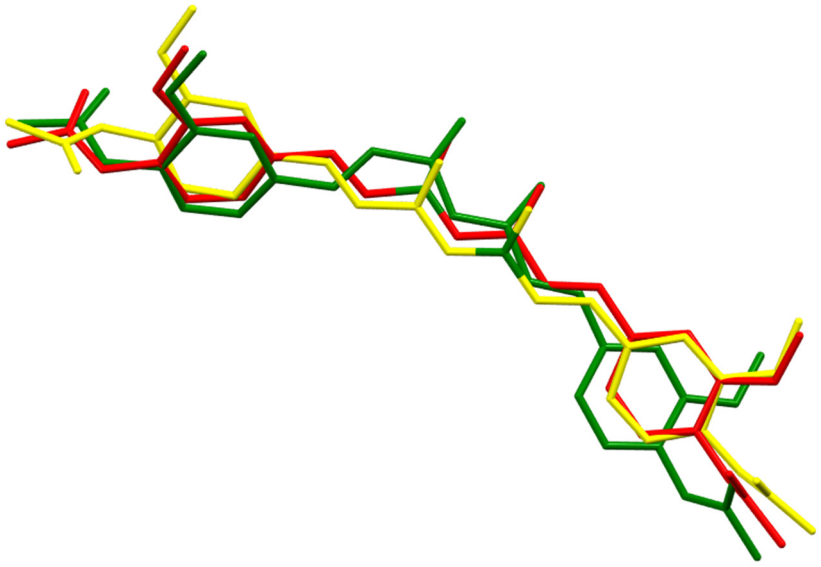

Figure 5. Molecular overlay of Diacetylcurcumin polymorphs: Color code; Form-1: red, Form-2: yellow and Form-3: green.

Intermolecular interactions such as C–H···O are weaker in the hydrogen bond hierarchy and are of secondary importance in directing the supramolecular assembly. However, in the absence of strong hydrogen bonds, weaker interactions can be major determinants of the overall crystal packing. Similarities and differences among the Forms 1, 2 and 3 of Diacetylcurcumin polymorphs the crystalline forms have been elucidated successfully using Hirshfeld surface, 2D fingerprinting, and intermolecular interaction analysis using the CrystalExplorer program. The surface analysis diagrams of the three crystal forms are shown in Figure 6.

The 2D fingerprint of intermolecular interactions indicates that the percentage contributions of H···H, C···H, and O···H contacts are similar. Among the three crystal forms, only the carbonyl oxygen atoms on the acetoxy group and the central keto–enol groups of DAC act as hydrogen-bond acceptors, forming O···H–C interactions, which are clearly visible as spikes. Besides the large portions of planar structures is notably the absence of π···π interactions, being the H···H, C···H, and O···H forces the main components (~70%) to the entire Hirshfeld surface.

The crystal packing in the polymorphs is constructed through the method 'energy frameworks' integrated in CrystalExplorer. All three DAC polymorphic forms show differences in the strength of interactions between the pair of molecules involved (Figure 7), and in all cases, the dispersion energy framework is dominant over the electrostatic energy framework, playing an important role in crystal packing arrangements, while their total interaction energies correlate well with their relative stability.

 doi:10.20944/preprints202605.1127.v1

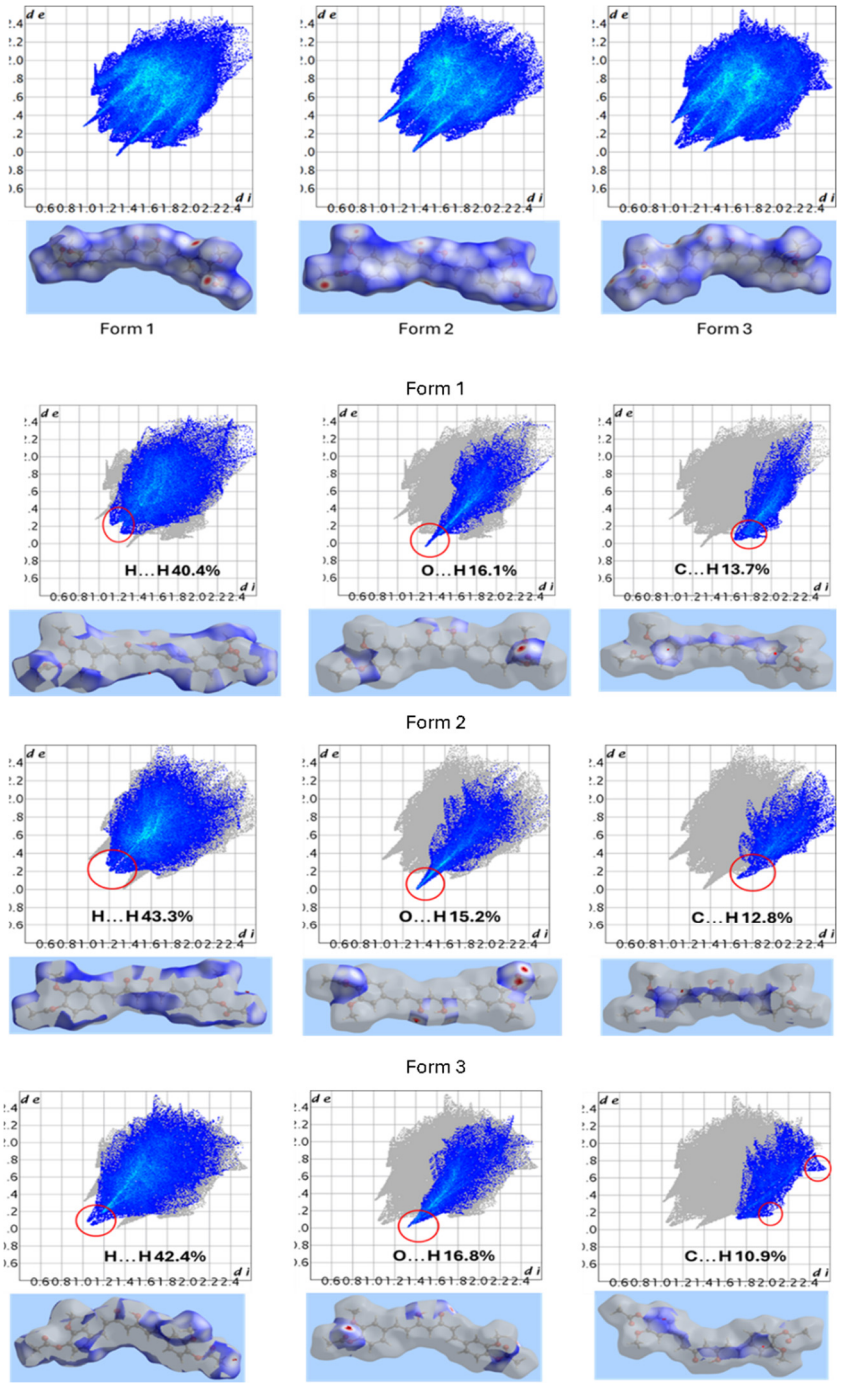

Figure 6. Principal contributions of intermolecular interactions to the Hirshfeld surface area are highlighted in red circles for Forms 1-3. The percentage of H…H, O…H and C…H interactions for molecules are indicated.

 doi:10.20944/preprints202605.1127.v1

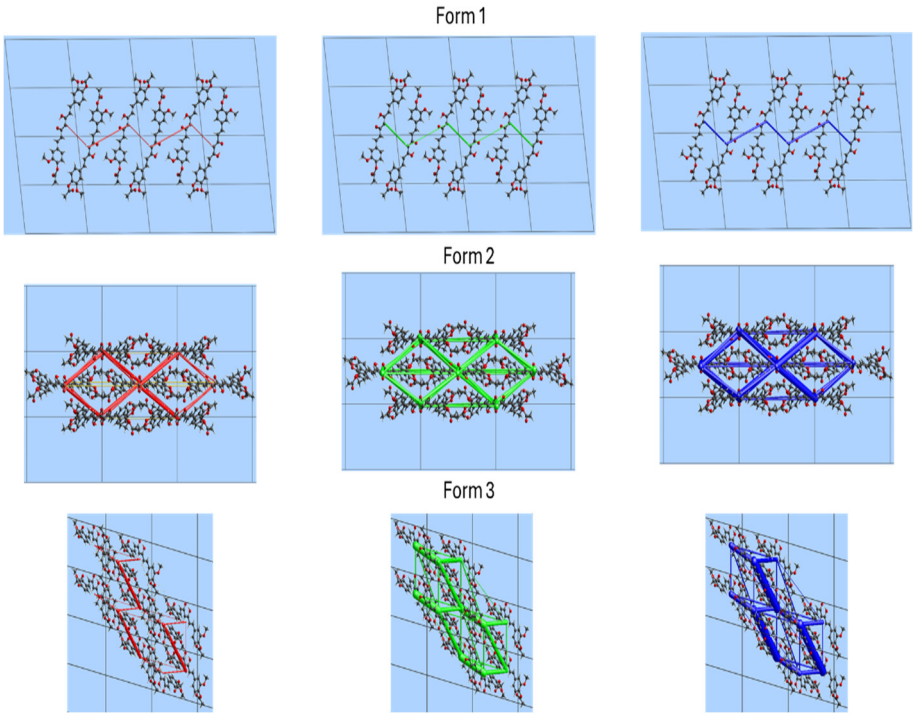

Figure 7. Energy framework diagrams viewed from the *a*-axis direction with energy scale factor of 100. Red: Coulomb energy; Green: Dispersion Energy and Blue: Total Energy.

The intermolecular energy calculations were performed with CrystalExplorer, and CLP-PIXEL programs (Table 7) and show that total energies on Form-1, Form-2, and Form-3 agree well with the thermal stability by the melting point. The energy calculations for DAC polymorphs are indicative that the most stable polymorph has a lower free energy [41] and the program that best correlates with the thermal study is CLP-PIXEL, indicating that the most stable crystallographic structure of Diacetylcurcumin is Form-3 (-262.2 kJ mol-1), metastable Form-1 (-247.6 kJ mol-1), and the most unstable is Form-2 (-245.4 kJ mol-1).

Table 7. Breakdown of Interaction energies (kJ mol-1) into Coulombic, polarization, dispersion, dipolar and repulsion components for the polymorphs of Diacetylcurcumin.

Polymorph	E_{coul}	E_{pol}	E_{dis}	Er_{ep}	E_{dip}	E_{tot}
			CystalExplorer			
Form-1	-38.9	-13.3	-189.9	74.7	-----	-170.3
Form-2	-73.1	-29	-293.6	105.1	-----	-289.5
Form-3	-83.9	-33.8	-347.8	110.4	-----	-348.3
			CLP-PIXEL			
Form 1	-35.5	-72.1	-205.5	67.1	-1.7	-247.6
Form 2	-43.9	-70.8	-196.8	66.1	-----	-245.4
Form 3	-46.0	-77.5	-214.5	75.8	-----	-262.2

It is surprising that Form-3 (considered the most stable) showed the lowest probability of crystallisation in the single-crystal formation tests by slow evaporation of a single solvent. This result correlates well with Ostwald's rule [42,43], as a low supersaturation rate allows sufficient time for a solute to reorganise and produce the growth of a more stable crystalline form.

 doi:10.20944/preprints202605.1127.v1

Form-3 was obtained by slow evaporation under refrigeration, using dichloromethane (10 days) and acetone (5 days) as solvents. This contrasts with crystallisation at room temperature (shorter evaporation time), which yields crystalline Form-1.

At a rapid supersaturation rate [44], kinetic effects predominate, explaining the discovery of the elusive polymorph (Form-2). In the crystallisation experiment with the solvent mixture using ethyl acetate and hexane (lower boiling point) under *vacuum*, high cooling or evaporation rates also occurred, resulting in the less stable polymorph (Form-2). Conversely, at a low supersaturation rate, thermodynamic effects prevail, which are suitable for the formation of the more stable Form-3.

The three DAC polymorphs were dissolved in a solvent mixture of ethanol (40%) and water. Although DAC is very insoluble in this medium, a direct correlation was found between solubility and stability. Form-2 is the most soluble (2.29×10^{-5} μM), the metastable Form-1 has intermediate solubility (1.20×10^{-5} μM), and Form-3 (1.16×10^{-5} μM) is the least soluble. Therefore, the stability of these polymorphs follows the order: Form 3 > Form 1 > Form 2.

4. Materials and Methods

All solvents and reagents were purchased from Sigma-Aldrich and used without further purification.

Five grams (13.57 mmol) of curcumin were dissolved in 100 mL of dichloromethane. Subsequently, 2.20 mL (27.14 mmol) of pyridine was added, followed by the addition of 2.2 equivalents of acetic anhydride (2.75 mL, 29.84 mmol). The reaction mixture was stirred magnetically overnight at room temperature. The solvent was then evaporated, and the residue was extracted with ethyl acetate (3 × 60 mL) and water. The organic phase was dried over anhydrous Na_2SO_4 and evaporated under reduced pressure. A yellow solid was obtained in 80% yield.

Approximately 100 mg of DAC powder was dissolved in 15 ml of a single solvent (with different dielectric constants [45]). These solutions were kept in slow evaporation at room temperature and protected from light. Once the appropriate crystalline medium was observed, the product was filtered through a Hirsch funnel and characterised by ATR-IR. The same procedure was applied for slow cold evaporation, except that a refrigerator set to 2 °C was used.

Approximately 100 mg of DAC powder was dissolved in 15 mL of a solvent (with different dielectric constants). Then, 10% of the corresponding anti-solvent (n-hexane or water) was added to each solution. These solutions were placed in a vacuum chamber (200 mbar) at room temperature, and rapid supersaturation of the medium was observed. Finally, the resulting product was filtered using a Hirsch funnel and characterized by ATR-IR spectroscopy.

^{1}H-NMR, ^{13}C-NMR, and two-dimensional spectra (HSQC and HMBC, see SI) were recorded on a Bruker Avance III 400 MHz spectrometer (Bruker, Rhein-stetten, Germany) using $CDCl_3$ as a solvent and TMS as reference, all spectra were processed using the MNova program [46].

HPLC (see SI) for DAC was performed as indicated in the literature [47] with minor modifications. Was recorded using an Agilent 1200 equipment with a detector of diodes-UV (see UV-spectrum for DAC in SI) Waters-2996 at 410 nm, solvent isocratic from acetonitrile/water 55:45 (orthophosphoric acid 0.02%), flow rate 1 mL/min, and Column Spherisorb 5 mm ODS1 250 X 4.6 mm as the stationary phase.

Infrared spectra were recorded on an FT-IR NICOLET IS-50 (Thermo Fisher Scien-tific, Waltham, MA, USA) using the attenuated total reflectance (ATR) technique (4000–400 cm−1).

Mass spectrum was recorded using the AccuTOF JMS-T100LC JEOL (JEOL de Mexico SA de CV, Mexico, CDMX) equipment for DART+, 350 °C, positive ion mode and calibration standard with PEG 600 [48]. The mass spectrum is shown in the supplementary material.

TGA and DSC analysis was carried out with a thermobalance TA Instruments, model Discovery 250 using an aluminum crucible, outer bottom Ø 5 mm. The sample was heated from 25 °C to 200 °C at a heating rate of 10 °C min−1 under nitrogen atmosphere [49].

13C CPMAS-NMR spectra were recorded using a Bruker 500 MHz spectrometer equipped with a probe PH MAS DVT (N-P/F/H).

 doi:10.20944/preprints202605.1127.v1

Crystal structure and refinement details. Intensity data were collected using a Bruker Apex diffractometer for Form-2 and Form-3 and a Bruker D8 Venture κ geometry diffractometer for Form-1. An absorption correction based on equivalent reflections was applied to the data. The structures were solved with the ShelXS [50] program and refined with ShelXL [51] managed in SHELXLe [52]. The models were refined using full-matrix least-squares minimisation on F2. Atomic hydrogen positions for those bonded to O atoms were located on a difference electron density map at an advanced refinement stage, while Hydrogen atomic positions for those bonded to C atoms were calculated from assumed geometries. Hydrogen atoms were included in structure factor calculations, but they were not refined. Isotropic displacement parameters of all the hydrogen atoms were approximated from the U(eq) value of the atom they were bonded to. The checkCIF/PLATON program was used to validate the structures, and the publication materials were prepared with CIFTAB and Mercury [53].

Solubility studies were performed in a mixture of water and ethanol (40%) [20]. 5 mg of polymorph 1, 2, or 3, were weighed and suspended in 5 mL of the solvent mixture. The suspension was kept under constant stirring for 24 hours. Subsequently, a 1 mL aliquot was taken and filtered through a 4-μm sintered filtration flask. From the filtrate, 100 microliters were taken and measured in triplicate at 410 nm in an ELISA microwell plate. The absorbance was then interpolated on the DAC standard curve in ethanol (see SI) to interpolar the micromolar concentration of each polymorph.

5. Conclusions

The polymorphic landscape of solid compounds can be explored through trial and error, though sometimes serendipity is required. Here, we rationally selected solvents and quickly analysed the resulting solids using ATR-IR. This approach reduced both time and money spent on analysis. Form-**2** (unstable) was obtained in solvents with the lowest dielectric constant, such as ethyl acetate/n-hexane, and rapid cooling by vacuum. Form-3 (more stable) was found in solvents with intermediate dielectric constant and longer crystallisation times. Form-1 (metastable) does not depend on a particular dielectric constant and appears in most solvents and conditions.

Herein, no crystallisation co-formers were used, so any co-crystallisation molecule is ruled out. To the best of our knowledge, this is the first example of acetylated curcumin polymorphs resulting from exhaustive ATR-IR scrutiny, and it is surprising to have experimentally observed a coincidence of three (the same as curcumin). With this experimental approach, it is expected that the time required to discover new polymorphic landscapes of other natural or synthetic curcuminoids will be shortened.

Supplementary Materials: The following supporting information can be downloaded at the website of this paper posted on Preprints.org. The crystallographic data for Form-1, Form-2 and Form-3 were deposited (including fcf files) in the Cambridge Crystallographic Data Centre (CCDC) with the Numbers 2490425 (Form-1), 2490426 (Form-2), 2490427 (Form-3). Table S1 shows the Crystal data and structure refinement of DAC polymorphs.

Author Contributions: Conceptualization, R.G.E.; methodology, M.A.O-M., R.T.H., R.S.O, C.E.M; software, R.G.E., R.A.T; validation, R.G.E., R.A.T. and M.A.O-M.; formal analysis, M.A.O-M., R.G.E.; investigation, M.A.O-M., R.T.H., R.S.O, C.E.M; resources, R.G.E.; data curation, R.G.E.; writing—original draft preparation, M.A.O-M., R.A.T, R.G.E.; writing—review and editing, M.A.O-M., R.T.H., R.S.O., R.A.T, R.G.E.; visualization, R.G.E.; supervision, R.G.E.; project administration, R.G.E.; funding acquisition, R.G.E. All authors have read and agreed to the published version of the manuscript.

Funding: DGAPA-PAPIIT-UNAM (IT202125) and SECIHTI (FOINS-PRONACES-307152).

Institutional Review Board Statement: Not applicable.

Informed Consent Statement: Not applicable.

Data Availability Statement: The data supporting this research can be obtained from the supplementary information (SI).

 doi:10.20944/preprints202605.1127.v1

Acknowledgments: RG Enríquez acknowledges support from DGAPA-PAPIIT-UNAM (IT202125) and SECIHTI (FOINS-PRONACES-307152). MA Obregón-Mendoza acknowledges support from SECITIH (postdoctoral fellowship, CVU- 599367). Rosario Tavera-Hernández acknowledges support from SECIHTI for their postdoctoral fellowship (CVU-662794). Acknowledgements are extended to Elizabeth Huerta (NMR), Isabel Chávez (NMR), Adriana Romo (ATR-IR), Martha Elena García Aguilera (^{13}C CP-MASS NMR, LURMN), María del Carmen García (MS), Eréndira García Ríos (HPLC), Lucero Ríos (HPLC), Antonio Nieto-Camacho (Solubility) and Alejandra Núñez Pineda (TGA) from the Instituto de Química, UNAM.

Conflicts of Interest: The authors declare no conflicts of interest.

References

1. Brog, J.P.; Chanez, C.L.; Crochet, A.; Fromm, K.M. Polymorphism, What It Is and How to Identify It: A Systematic Review. *RSC Adv.* 2013, *3*, 16905–16931.
2. Nangia, A. Conformational Polymorphism in Organic Crystals. *Acc. Chem. Res.* 2008, *41*, 595–604, doi:10.1021/ar700203k.
3. Bernstein, J. Polymorphism - A Perspective. *Cryst. Growth Des.* 2011, *11*, 632–650, doi:10.1021/cg1013335.
4. Braga, D.; Grepioni, F.; Maini, L. The Growing World of Crystal Forms. *Chemical Communications* 2010, *46*, 6232–6242.
5. Gupta, S.C.; Prasad, S.; Kim, J.H.; Patchva, S.; Webb, L.J.; Priyadarsini, I.K.; Aggarwal, B.B. Multitargeting by Curcumin as Revealed by Molecular Interaction Studies. *Nat. Prod. Rep.* 2011, *28*, 1937–1955, doi:10.1039/c1np00051a.
6. Witika, B.A.; Makoni, P.A.; Matafwali, S.K.; Mweetwa, L.L.; Shandele, G.C.; Walker, R.B. Enhancement of Biological and Pharmacological Properties of an Encapsulated Polyphenol: Curcumin. *Molecules* 2021, *26*, 1–19, doi:10.3390/molecules26144244.
7. Pfund, L.Y.; Matzger, A.J. Towards Exhaustive and Automated High-Throughput Screening for Crystalline Polymorphs. *ACS Comb. Sci.* 2014, *16*, 309–313, doi:10.1021/co500043q.
8. Chainoglou, E.; Siskos, A.; Pontiki, E.; Hadjipavlou-Litina, D. Hybridization of Curcumin Analogues with Cinnamic Acid Derivatives as Multi-Target Agents Against Alzheimer's Disease Targets. *Molecules* 2020, *25*, doi:10.3390/molecules25214958.
9. Sanphui, P.; Bolla, G. Curcumin, a Biological Wonder Molecule: A Crystal Engineering Point of View. *Cryst. Growth Des.* 2018, *18*, 5690–5711, doi:10.1021/acs.cgd.8b00646.
10. Kunnumakkara, A.B.; Anand, P.; Aggarwal, B.B. Curcumin Inhibits Proliferation, Invasion, Angiogenesis and Metastasis of Different Cancers through Interaction with Multiple Cell Signaling Proteins. *Cancer Lett.* 2008, *269*, 199–225, doi:10.1016/j.canlet.2008.03.009.
11. Gano, M.; Klebeko, J.; Pełech, R. Efficient Esterification of Curcumin in Bis(Trifluoromethylsulfonyl)Imide-Based Ionic Liquids. *J. Mol. Liq.* 2021, *337*, doi:10.1016/j.molliq.2021.116420.
12. Souza, V. de; Polaquini, C.R.; de Moraes, G.R.; Oliveira Braga, A.R.; da Silva, P.V.; da Silva, D.R.; Ribeiro Lima, F.R.; Regasini, L.O.; Cássia Orlandi Sardi, J. de Diacetylcurcumin: A Novel Strategy against Enterococcus Faecalis Biofilm in Root Canal Disinfection. *Future Microbiol.* 2024, *19*, 647–654, doi:10.2217/fmb-2023-0235.
13. Mohammadi, F.; Bordbar, A.K.; Divsalar, A.; Mohammadi, K.; Saboury, A.A. Analysis of Binding Interaction of Curcumin and Diacetylcurcumin with Human and Bovine Serum Albumin Using Fluorescence and Circular Dichroism Spectroscopy. *Protein Journal* 2009, *28*, 189–196, doi:10.1007/s10930-009-9184-1.
14. Mohammadi, F.; Moeeni, M. Investigation of the Binding Interactions of Bisdemethoxycurcumin, Diacetylcurcumin and Diacetylbisdemethoxycurcumin with Bovine α-Lactalbumin by Experimental and Theoretical Analysis. *J. Biomol. Struct. Dyn.* 2017, *35*, 3486–3498, doi:10.1080/07391102.2016.1259588.
15. Escobedo-Martínez, C.; Guzmán-Gutiérrez, S.L.; Carrillo-López, M.I.; Deveze-Álvarez, M.A.; Trujillo-Valdivia, A.; Meza-Morales, W.; Enríquez, R.G. Diacetylcurcumin: Its Potential Antiarthritic Effect on a Freund's Complete Adjuvant-Induced Murine Model. *Molecules* 2019, *24*, 2643, doi:10.3390/molecules24142643.

 doi:10.20944/preprints202605.1127.v1

16. Basile, V.; Ferrari, E.; Lazzari, S.; Belluti, S.; Pignedoli, F.; Imbriano, C. Curcumin Derivatives: Molecular Basis of Their Anti-Cancer Activity. *Biochem. Pharmacol.* 2009, *78*, 1305–1315, doi:10.1016/j.bcp.2009.06.105.
17. Sardi, J. de C.O.; Polaquini, C.R.; Freires, I.A.; Galvão, L.C. de C.; Lazarini, J.G.; Torrezan, G.S.; Regasini, L.O.; Rosalen, P.L. Antibacterial Activity of Diacetylcurcumin against Staphylococcus Aureus Results in Decreased Biofilm and Cellular Adhesion. *J. Med. Microbiol.* 2017, *66*, 816–824, doi:10.1099/jmm.0.000494.
18. Sanches, C.V.G.; Sardi, J. de C.O.; Terada, R.S.S.; Lazarini, J.G.; Freires, I.A.; Polaquini, C.R.; Torrezan, G.S.; Regasini, L.O.; Fujimaki, M.; Rosalen, P.L. Diacetylcurcumin: A New Photosensitizer for Antimicrobial Photodynamic Therapy in Streptococcus Mutans Biofilms. *Biofouling* 2019, *35*, 340–349, doi:10.1080/08927014.2019.1606907.
19. Hjorth Tonnesen, H.; Karlsen, J.; Mostad, A. Structural Studies of Curcuminoids. I. The Crystal Structure of Curcumin. *Acta Chemica Scandinavica B* 1982, *36*, 475–479.
20. Sanphui, P.; Goud, N.R.; Khandavilli, U.B.R.; Bhanoth, S.; Nangia, A. New Polymorphs of Curcumin. *Chemical Communications* 2011, *47*, 5013–5015, doi:10.1039/c1cc10204d.
21. Lv, R.; Zhang, X.; Xing, R.; Shi, W.; Zhao, H.; Li, W.; Jouyban, A.; Acree, W.E. Comprehensive Understanding on Solubility and Solvation Performance of Curcumin (Form I) in Aqueous Co-Solvent Blends. *Journal of Chemical Thermodynamics* 2022, *167*, doi:10.1016/j.jct.2021.106718.
22. Matlinska, M.A.; Wasylishen, R.E.; Bernard, G.M.; Terskikh, V. V.; Brinkmann, A.; Michaelis, V.K. Capturing Elusive Polymorphs of Curcumin: A Structural Characterization and Computational Study. *Cryst. Growth Des.* 2018, *18*, 5556–5563, doi:10.1021/acs.cgd.8b00859.
23. Horosanskaia, E.; Yuan, L.; Seidel-morgenstern, A.; Lorenz, H. Purification of Curcumin from Ternary Extract-Similar Mixtures of Curcuminoids in a Single Crystallization Step. *Crystals (Basel).* 2020, *10*, doi:10.3390/cryst10030206.
24. Pandey, K.U.; Dalvi, S.V. Understanding Stability Relationships among Three Curcumin Polymorphs. *Advanced Powder Technology* 2019, *30*, 266–276, doi:10.1016/j.apt.2018.11.002.
25. Mague, J.T.; Alworth, W.L.; Payton, F.L. Curcumin and Derivatives. *Acta Crystallogr. C* 2004, *60*, doi:10.1107/S0108270104015434.
26. Meza-Morales, W.; Mirian Estévez-Carmona, M.; Alvarez-Ricardo, Y.; Obregón-Mendoza, M.A.; Cassani, J.; Ramírez-Apan, M.T.; Escobedo-Martínez, C.; Soriano-García, M.; Reynolds, W.F.; Enríquez, R.G. Full Structural Characterization of Homoleptic Complexes of Diacetylcurcumin with Mg, Zn, Cu, and Mn: Cisplatin-Level Cytotoxicity in Vitro with Minimal Acute Toxicity in Vivo. *Molecules* 2019, *24*, doi:10.3390/molecules24081598.
27. Mohammadi, K.; Thompson, K.H.; Patrick, B.O.; Storr, T.; Martins, C.; Polishchuk, E.; Yuen, V.G.; McNeill, J.H.; Orvig, C. Synthesis and Characterization of Dual Function Vanadyl, Gallium and Indium Curcumin Complexes for Medicinal Applications. *J. Inorg. Biochem.* 2005, *99*, 2217–2225, doi:10.1016/j.jinorgbio.2005.08.001.
28. Bond, A.D. Polymorphism in Molecular Crystals. *Curr. Opin. Solid State Mater. Sci.* 2009, *13*, 91–97, doi:10.1016/j.cossms.2009.06.004.
29. Alvarez-Ricardo, Y.F.; Sánchez-López, D.M.; Meza-Morales, W.E.; Obregón-Mendoza, M.A.; Arias-Olguín, I.I.; Nieto-Camacho, A.; Toscano, R.A.; Enríquez, R.G. Stereochemistry and Antioxidant Activity of 1,3-Diol Derivatives of Diacetylcurcumin-4H: A Joint NMR, X-Ray, and Biological Approach. *ChemistrySelect* 2020, *5*, 1616–1622, doi:10.1002/slct.201903089.
30. Ukrainczyk, M.; Hodnett, B.K.; Rasmuson, Å.C. Process Parameters in the Purification of Curcumin by Cooling Crystallization. *Org. Process Res. Dev.* 2016, *20*, 1593–1602, doi:10.1021/acs.oprd.6b00153.
31. Sanphui, P.; Goud, N.R.; Khandavilli, U.B.R.; Nangia, A. Fast Dissolving Curcumin Cocrystals. *Cryst. Growth Des.* 2011, *11*, 4135–4145, doi:10.1021/cg200704s.
32. Chieng, N.; Rades, T.; Aaltonen, J. An Overview of Recent Studies on the Analysis of Pharmaceutical Polymorphs. *J. Pharm. Biomed. Anal.* 2011, *55*, 618–644.
33. Harris, R.K. Applications of Solid-State NMR to Pharmaceutical Polymorphism and Related Matters. *Journal of Pharmacy and Pharmacology* 2010, *59*, 225–239, doi:10.1211/jpp.59.2.0009.
34. Payton, F.; Sandusky, P.; Alworth, W.L. NMR Study of the Solution Structure of Curcumin. *J. Nat. Prod.* 2007, *70*, 143–146, doi:10.1021/np060263s.

 doi:10.20944/preprints202605.1127.v1

35. Meza-Morales, W.; Alvarez-Ricardo, Y.; Obregón-Mendoza, M.A.; Arenaza-Corona, A.; Ramírez-Apan, M.T.; Toscano, R.A.; Poveda-Jaramillo, J.C.; Enríquez, R.G. Three New Coordination Geometries of Homoleptic Zn Complexes of Curcuminoids and Their High Antiproliferative Potential. *RSC Adv.* 2023, *13*, 8577–8585, doi:10.1039/d3ra00167a.
36. Mukhopadhyay, A.; Basu, N.; Ghatak, N.; Gujral, P.K. Anti-Inflammatory and Irritant Activities of Curcumin Analogues in Rats. *Agents Actions* 1982, *12*, 4.
37. Liu, B.; Xia, M.; Ji, X.; Xu, L.; Dong, J. *Synthesis and Antiproliferative Effect of Novel Curcumin Analogues*; 2013; Vol. 61;.
38. Dai, Y.; Terskikh, V.; Brinmkmann, A.; Wu, G. Solid-State 1H, 13C, and 17O NMR Characterization of the Two Uncommon Polymorphs of Curcumin. *Cryst. Growth Des.* 2020, *20*, 7484–7491, doi:10.1021/acs.cgd.0c01164.
39. Cruz-Cabeza, A.J.; Bernstein, J. Conformational Polymorphism. *Chem. Rev.* 2014, *114*, 2170–2191.
40. Cruz-Cabeza, A.J.; Reutzel-Edens, S.M.; Bernstein, J. Facts and Fictions about Polymorphism. *Chem. Soc. Rev.* 2015, *44*, 8619–8635.
41. Bernstein, J.; Davey, R.J.; Henk, J.-O. Concomitant Polymorphs. *Angew. Chem. Inter. Ed.* 1999, *38*, 3440–3461, doi:10.1002/(SICI)1521-3773(19991203).
42. Cruz-Cabeza, A.J.; Feeder, N.; Davey, R.J. Open Questions in Organic Crystal Polymorphism. *Commun. Chem.* 2020, *3*.
43. Bučar, D.; Lancaster, R.W.; Bernstein, J. Disappearing Polymorphs Revisited. *Angewandte Chemie* 2015, *127*, 7076–7098, doi:10.1002/ange.201410356.
44. Heffernan, C.; Soto, R.; Hodnett, B.K.; Rasmuson, Å.C. Growth Kinetics of Curcumin Form I. *CrystEngComm* 2020, *22*, 3505–3518, doi:10.1039/d0ce00034e.
45. Nangia, A.; Desiraju, G.R. *Pseudopolymorphism: Occurrences of Hydrogen Bonding Organic Solvents in Molecular Crystals*; 1998;
46. Mestrelab Research. MNova Software. Available Online Https://Mestrelab.Com/Download/Mnova/ (Accesed on March, 10, 2024).
47. Jayaprakasha, G.K.; Rao, L.J.M.; Sakariah, K.K. Improved HPLC Method for the Determination of Curcumin, Demethoxycurcumin, and Bisdemethoxycurcumin. *J. Agric. Food Chem.* 2002, *50*, 3668–3672, doi:10.1021/jf025506a.
48. Obregón-Mendoza, M.A.; Arias-Olguín, I.I.; Estévez-Carmona, M.M.; Meza-Morales, W.; Alvarez-Ricardo, Y.; Toscano, R.A.; Arenas-Huertero, F.; Cassani, J.; Enríquez, R.G. Non-Cytotoxic Dibenzyl and Difluoroborate Curcuminoid Fluorophores Allow Visualization of Nucleus or Cytoplasm in Bioimaging. *Molecules* 2020, *25*.
49. Obregón-Mendoza, M.A.; Meza-Morales, W.; Rodríguez-Hernández, K.D.; Estévez-Carmona, M.M.; Pérez-González, L.L.; Tavera-Hernández, R.; Ramírez-Apan, M.T.; Barrera-Hernández, D.; García-Olivares, M.; Monroy-Torres, B.; et al. The Antitumoral Effect In Ovo of a New Inclusion Complex from Dimethoxycurcumin with Magnesium and Beta-Cyclodextrin. *Int. J. Mol. Sci.* 2024, *25*.
50. Sheldrick, G.M. A Short History of SHELX. *Acta Crystallogr. A* 2015, *64*, 112–122, doi:10.1107/S0108767307043930.
51. Sheldrick, G.M. Crystal Structure Refinement with SHELXL. *Acta Crystallogr. A* 2015, *71*, 3–8, doi:10.1107/S2053273314026370.
52. Hübschle, C.B., S.G.M., D.B. ShelXle: A Qt Graphical User Interface for SHELXL. *J. Appl.Cryst* 2011, *44*, 1281–1284.
53. Macrae, C.F.; Sovago, I.; Cottrell, S.J.; Galek, P.T.A.; McCabe, P.; Pidcock, E.; Platings, M.; Shields, G.P.; Stevens, J.S.; Towler, M.; et al. Mercury 4.0: From Visualization to Analysis, Design and Prediction. *J. Appl. Crystallogr.* 2020, *53*, 226–235, doi:10.1107/S1600576719014092.